

Efficient Defect Passivation for Perovskite Solar Cells by Controlling the Electron Density Distribution of Donor- π -Acceptor Molecules

Tianhao Wu, Yanbo Wang, Xing Li, Yongzhen Wu, Xiangyue Meng, Danyu Cui, Xudong Yang, and Liyuan Han*

Organic–inorganic hybrid perovskite solar cells (PSCs) are a promising photovoltaic technology that has rapidly developed in recent years. Nevertheless, a large number of ionic defects within perovskite absorber can serve as non-radiative recombination center to limit the performance of PSCs. Here, organic donor- π -acceptor (D- π -A) molecules with different electron density distributions are employed to efficiently passivate the defects in the perovskite films. The X-ray photoelectron spectroscopy (XPS) analysis shows that the strong electron donating N,N-dibutylaminophenyl unit in a molecule causes an increase in the electron density of the passivation site that is a carboxylate group, resulting in better binding with the defects of under-coordinated Pb^{2+} cations. Carrier lifetime in the perovskite films measured by the time-resolved photoluminescence spectrum is also prolonged by an increase in donation ability of the D- π -A molecules. As a consequence, these benefits contribute to an increase of 80 mV in the open circuit voltage of the devices, enabling a maximum power conversion efficiency (PCE) of 20.43%, in comparison with PCE of 18.52% for the control device. The authors' findings provide a novel strategy for efficient defect passivation in the perovskite solar cells based on controlling the electronic configuration of passivation molecules.

400–800 nm,^[1–3] adjustable band gap from 1.4 to 1.6 eV,^[4,5] long diffusion length for charge carriers and low-temperature crystallization process make it an inherent material for solar cells application,^[6–8] attracting much attention from all over the world.^[9–12] For now, the highest certified efficiency of perovskite solar cells (PSCs) has exceeded 23%,^[13] which is comparable with silicon solar cells and the commercialization of PSCs is worth expecting. However, the perovskite films currently fabricated by the solution deposition process show a polycrystalline structure with a large number of ionic defects at the surface and grain boundaries (GBs).^[14,15] These defects can not only serve as non-radiative recombination center contributing to a major energy loss mechanism, but also create fast channels for the permeation of moisture or oxygen, which is detrimental to the stability of perovskite devices. Therefore, effective passivation method is in urgent need to further

1. Introduction

Low-cost organometal halide perovskite materials with strong light-absorption coefficient in the wavelength between


enhance the efficiency and prolong the durability of PSCs.

So far, many efforts have been done to enlarge the grain size of polycrystalline films, reducing the total area of GBs,^[16–19] or to optimize the interface band alignment between perovskite and charge transport layers to prevent the carriers from falling in surface defects and trap states.^[20–23] These passivation strategies significantly suppress the charge recombination and increase the carrier lifetime in perovskite films. Nevertheless, challenges still remain such as the small energy barrier for ion migration under thermal or illuminated activation causing a non-stoichiometry decomposition of the perovskite crystal,^[24–26] which promotes the formation of halide vacancies and under-coordinated Pb^{2+} ions that are regarded as the main source of electronic trap states in the perovskite film.^[27,28] Previous studies demonstrated that many molecules such as guanidinium, iodopentafluorobenzene, pyridine, thiophene, and carboxyl derivatives can heal the trap states by forming coordination with the under-coordinated Pb^{2+} cations or halide anions,^[29–31] resulting in an order of magnitude increase in the photoluminescence (PL) lifetime of perovskite absorber.^[32] These works implicate that the electron configuration of molecular additive play a vital role in the defects passivation process

Dr. T. Wu, Dr. Y. Wang, Dr. D. Cui, Prof. X. Yang, Prof. L. Han
State Key Laboratory of Metal Matrix Composites
Shanghai Jiao Tong University
800 Dong Chuan Road, Shanghai 200240, China
E-mail: Han.liyuan@sjtu.edu.cn

Dr. X. Meng, Prof. L. Han
Research Network and Facility Services Division
National Institute for Materials Science
Tsukuba, Ibaraki 305-0047, Japan

Dr. X. Li, Dr. Y. Wu
Key Laboratory for Advanced Materials
Joint International Research Laboratory of Precision Chemistry
and Molecular Engineering
School of Chemistry and Molecular Engineering
East China University of Science and Technology
Shanghai 200237, China

 The ORCID identification number(s) for the author(s) of this article can be found under <https://doi.org/10.1002/aenm.201803766>.

DOI: 10.1002/aenm.201803766

and improving the performance of perovskite solar cells by increase in open circuit voltage. However, rare work is detailed with a comprehensive study to understand design rule for the passivation molecules.

In other words, organic D- π -A molecules composed of an electron donor, a π -spacer, and an electron acceptor exhibit the superiorities of simple synthetic method, good stability, and flexible electron density distribution by adjusting their electron-donating substituents or electron-withdrawing functional groups.^[33,34] These advantages make it convenient for the research on discovering design rules for efficient passivators. Typically, as donor parts, many aromatic systems with electron-donating ability such as triarylamines, indolines, carbazoles, dithienothiophenes, phenoxazines are employed.^[35] Counterpart acceptor parts are designed with electron-withdrawing functional groups, generally, cyano, carboxyl, trifluoromethyl, rhodamine, nitril, and pyridine being frequently used.^[36,37] As π -spacer units, π -conjugated systems such as polyene, furan, pyrrole, thiophene, benzothiadiazole, and benzotriazole are incorporated into the D- π -A molecules to keep the molecular planarity and promote the electron delocalization through overlapping π -orbitals.^[38]

In this study, we employ three organic D- π -A molecules (SP1, SP2, SP3) designed with different substituted phenyl units as the electron donor to passivate the ionic defects within MAPbI₃ perovskite. The π -spacer and acceptor parts are thiophene and cyanoacetic acid, respectively (Figure 1a). It was demonstrated that the passivation effect increases with the polarity of the D- π -A molecules. The strong electron-donating N,N-dibutylaminophenyl unit on the donor part would significantly increase the electron density on the carboxylate end group and make it much more electron-rich.^[39–41] Such dipolar electron density distribution of SP3 provides better conditions for coordination or binding with the under-coordinated Pb²⁺ defects, as compared to that of the SP1 and SP2 with weakly electron-donating phenyl and butoxyphenyl units, respectively. The results demonstrated that the introduction of SP3 effectively eliminated the metallic Pb cluster caused by under-coordinated Pb²⁺ defect on the perovskite surface, resulting in minimizing the electronic trap states in perovskite layer and enhance the performance of PSCs. Consequently, the PSCs with an inverted planar structure passivated with SP3 exhibited an increase of 80 mV in Voc, significantly enhancing the power conversion efficiency (PCE) from 18.52% to 20.43%. In addition, the SP3 passivated perovskite devices displayed a remarkable improvement in air stability. The solar cell encapsulated retains 86% of its initial PCE after 30 days aging in ambient air, while the control device underwent a 37% decrease of the initial PCE. These results emphasize the importance of electronic configuration of passivation molecules for enhancing both efficiency and stability of PSCs devices.

2. Results and Discussion

SP1, SP2, and SP3 molecules are synthesized according to the other reports,^[39] and the detailed information is depicted in Figure S1, Supporting Information. To visualize the electron density distribution in corresponding D- π -A molecules, we

perform the electrostatic potential (ESP) analysis (Figure 1b) calculated from the density functional theory (DFT) method. As shown in Figure 1b, the electron-deficient area (positive area) mainly distributes on the site of electron-donating substituents connected on the phenyl rings. On the other hand, the electron-withdrawing end group of carboxylate (O = C–O) on the acceptor part presents a high electron density (negative area), providing favorable condition for coordination with the under-coordinated Pb²⁺ cations, as depicted in Figure 1c. This dipolar charge distribution is much more obvious in the case of SP3, attributed to the effective coupling of molecules orbitals between the nitrogen site of N,N-dibutylamine substituent and the π -conjugated system, causing a strong electron delocalization from the donor part to the acceptor part (Figure S2, Supporting Information). Such effect could further enhance the interaction between SP3 and the under-coordinated ionic defects presented in perovskite crystal.

Defect passivation of perovskite layer is conducted through an in situ solvent engineering route during the one-step solution deposition process. We added D- π -A molecules into the antisolvent (chlorobenzene) and dripped it on the perovskite precursor (PbI₂ + MAI) before the crystallization of perovskite film under thermal annealing. The detailed procedure is provided in the experimental section. **Furthermore, time-of-flight secondary-ion mass spectrometry (TOF-SIMS) analysis illustrates that the D- π -A molecules (indicated by S⁻) mainly locate on the upper part of perovskite layer (indicated by PbI⁻), especially the top surface (Figure S3, Supporting Information).** The coordinated reaction between the carboxylate (O = C–O) of D- π -A molecules and the Pb²⁺ cation was demonstrated by the Fourier transform infrared (FTIR) spectroscopy characterization. Figure S4, Supporting Information, shows the FTIR spectra of SP3 and PbI₂-SP3 mixture. The stretching vibration of C = O bond in pure SP3 was observed at 1706 cm⁻¹, while the C = O vibration was shifted to a lower wavenumber of 1691 cm⁻¹ in the PbI₂-SP3 sample. In addition, Figure S5, Supporting Information, compares the surface scanning electron microscopy (SEM) image of the corresponding perovskite samples, indicating the introduction of D- π -A molecules has negligible impact on the surface morphology and grain size of perovskite films. The X-ray diffraction (XRD) patterns shown in Figure S6, Supporting Information, confirmed that large-size D- π -A molecules could not permeate into the perovskite crystal to induce a phase transition or form certain 2D structure on the surface and GBs of perovskite films.

Additionally, we employed the X-ray photoelectron spectroscopy (XPS) to detect the surface coordinated condition of the Pb element in MAPbI₃ perovskite before and after passivation. Figure 1d shows the surface Pb 4f core level of the corresponding perovskite samples, where the dominating peaks (138.3 eV for 4f_{7/2} and 143.2 eV for 4f_{5/2}) are associated with the Pb²⁺ components with a saturated coordination, and the small peaks at lower binding energy (136.8 eV for 4f_{7/2} and 141.7 eV for 4f_{5/2}) are attributed to the defect of under-coordinated Pb²⁺ ion that has recently been assigned to the metallic Pb cluster (Pb⁰), which could be attributed to the fact that highly under-coordinated Pb may exhibit a metallic characteristic.^[42,43] After the introduction of D- π -A molecules, we found that the Pb⁰ components drop obviously and almost disappear in the case of SP3, which can

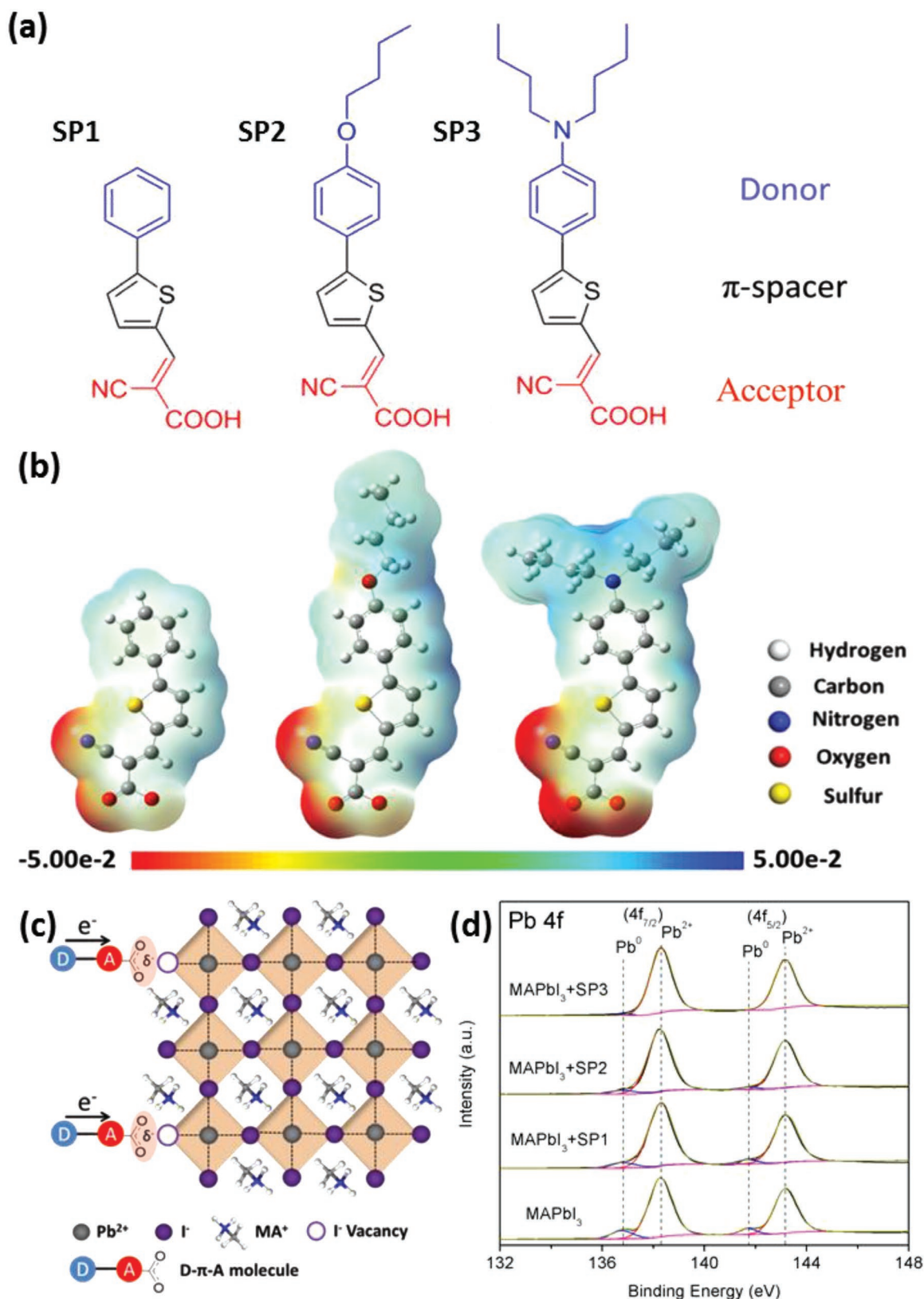


Figure 1. a) Chemical structures of SP1, SP2, and SP3. b) Calculated ESP profiles of SP1, SP2, and SP3. c) Schematic illustration of the passivation process of D- π -A molecules for the under-coordinated Pb^{2+} cations. d) XPS Pb 4f core level of the MAPbI₃ perovskite films without and with the passivation of SP1, SP2, and SP3 deposited on the NiO_x-coated FTO substrate.

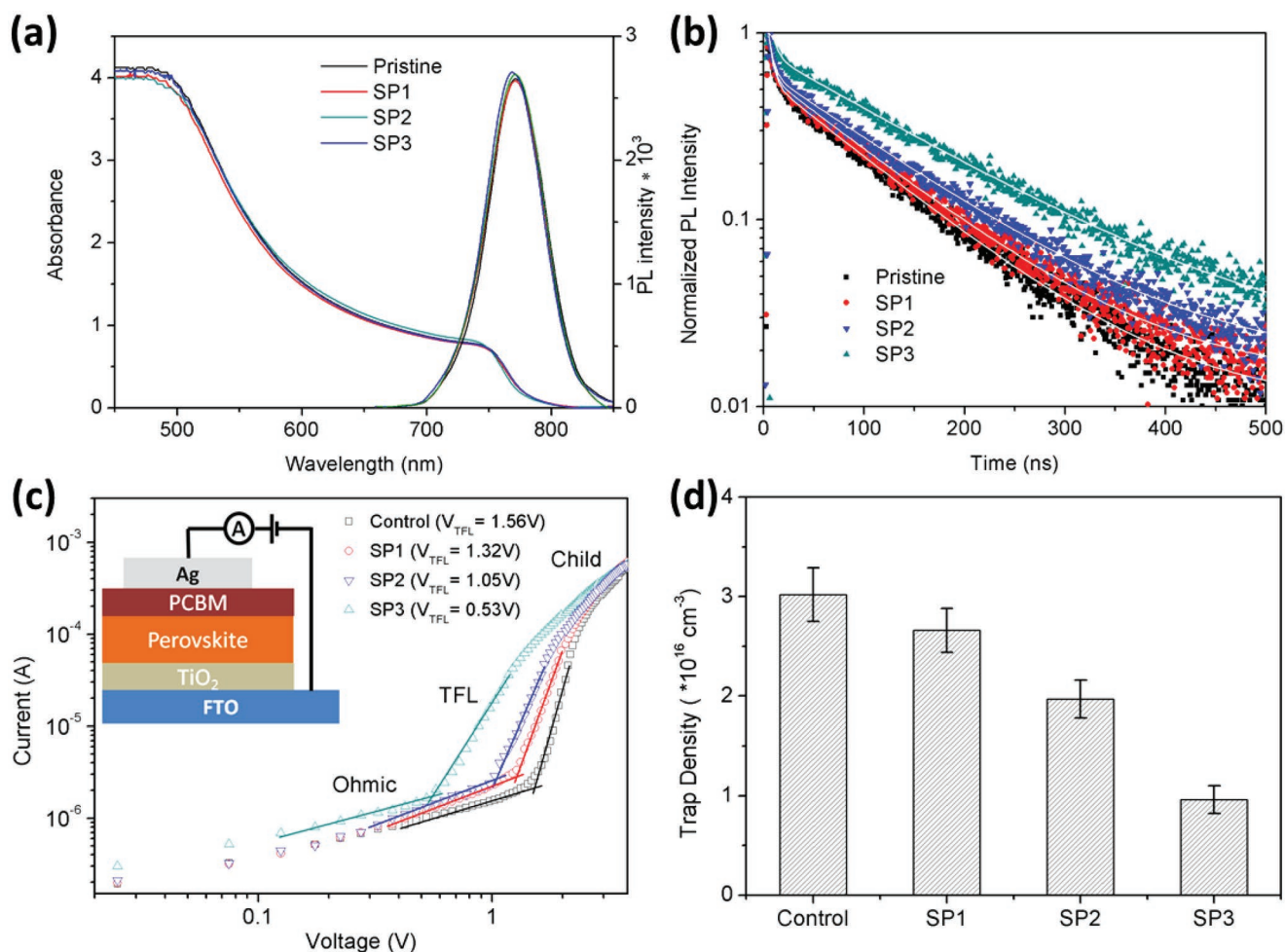


Figure 2. a) UV-vis absorption spectrum and steady state PL spectrum of the corresponding perovskite films deposited on bare glass substrate. b) Time-resolved PL decay of the corresponding perovskite films deposited on the bare glass substrate using a 370 nm excitation light source. c) The representative dark I-V plots of the electron-only perovskite devices, the device structure is shown in the inset. Three regions can be identified according to different values of the slope n : $n = 1$ is the Ohmic region, $n = 2$ is the SCLC region (Child), and $n > 2$ is the trap-filled limited region (TFL). d) Statistic trap density for the control and passivated perovskite films based on 10 testing devices derived from the SCLC measurement.

be interpreted as the result of better coordination effect forming between the Pb^{2+} cation and the carboxylate functional group with much higher electron density incorporated on the cyanoacetic acid unit. The intensive coordination effect of SP3 was verified by the increasing intensity of Pb-O component at 529.4 eV with a weakened peak intensity of C = O bond at 531.5 eV in comparison with SP1 and SP2, as illustrated in the XPS O 1s spectrums (Figure S7, Supporting Information).^[44] Besides, we also found that the UV-vis absorption peaks show a strong blue shift in the SP3-PbI₂ complex (1:1 in molar ratio) but depict negligible change for SP1-PbI₂ SP2-PbI₂ mixtures, as shown in Figure S8, Supporting Information. Such effect could be ascribed to the strong coordinated reaction with Pb^{2+} cations weakening the C = O bond of cyanoacetic acid, which leads to a partial break of the π -conjugated system and thus alters the intramolecular charge-transfer absorption band of the D- π -A molecule.^[40]

Furthermore, we investigate the impact of passivation treatment on the optical and electronic properties of perovskite films. The UV-vis spectrum shown in Figure 2a implies that the presence of D- π -A molecules does not affect the UV-vis

absorption of the perovskite materials. Besides, the steady-state PL spectra indicate that defect-mitigated process has little influence on the band gap of perovskite film. Figure 2b depicts the time-resolved PL plots of the corresponding perovskite samples deposited on the bare glass substrate. The PL decay curves are fitted with double exponential equation, and the derived parameters are summarized in Table S1, Supporting Information. The fitting result shows that the fast decay lifetime (τ_1) accounting for the biomolecular recombination of photo-generated free carriers is not obviously changed by the passivation process, and the slow decay lifetime (τ_2) associated with the trap-assisted recombination exhibits a much higher value of 142.7 ns for the SP3 passivated perovskite, compared with the pristine (99.8 ns), SP1 passivated (105.9 ns), and SP2 passivated (116.5 ns) ones. As known, the enhanced PL lifetime means less non-radiative recombination and lower trap density, suggesting that SP3 is the most effective passivator in reducing the trap states of perovskite films. Additionally, time-resolved PL spectrums of the PCBM-coated perovskite films before and after passivation show little difference in the PL decay lifetime,

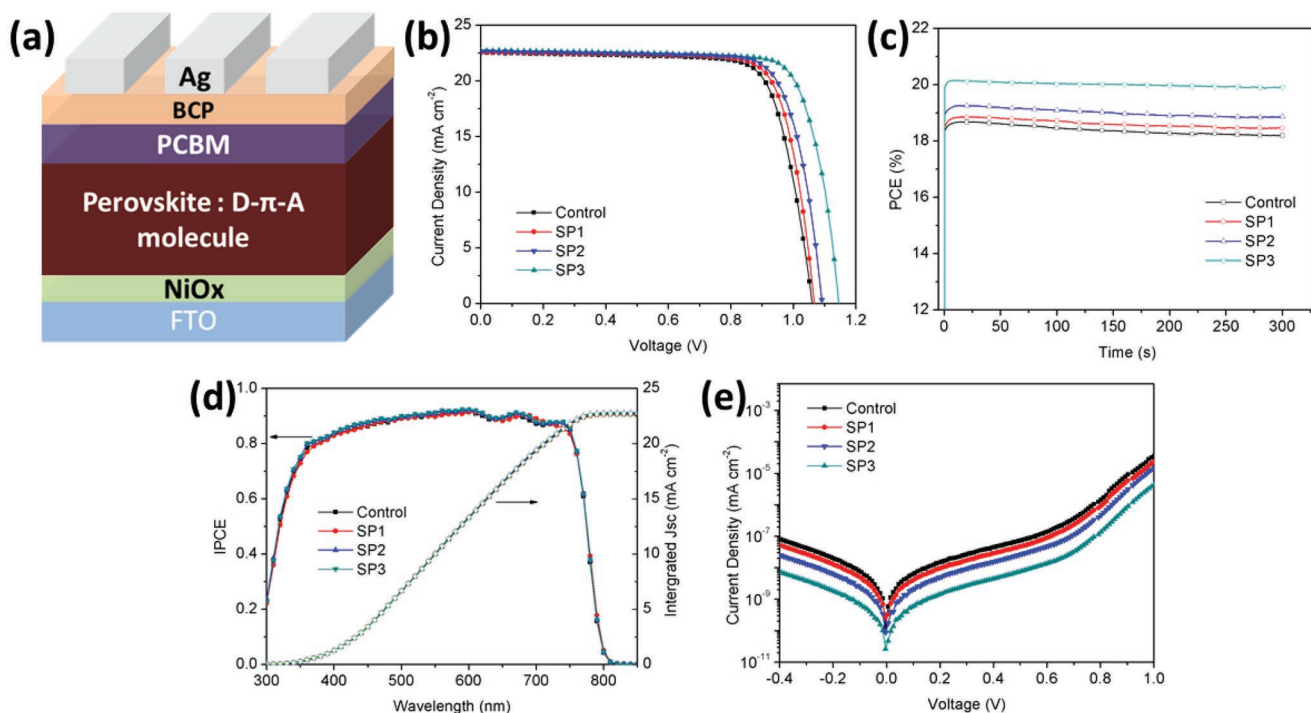


Figure 3. a) Device structure diagram of the PSCs. b) J - V characteristic of the champion devices with a 0.09 cm^2 effective cell area under simulated AM 1.5G solar illumination based of different perovskite absorbers. c) Steady-state PCE measured under maximum power point tracking for 300 s of the champion device without and with the passivation of D- π -A molecules. d) Internal photo-to-current efficiency (IPCE) together with the corresponding integrated current density of the champion device without and with the passivation of D- π -A molecules. e) Dark J - V measurements for the champion device without and with the passivation of D- π -A molecules.

as illustrated in Figure S9, Supporting Information, implying the D- π -A molecules presented on perovskite surface have negligible impact on the interface charge extraction efficiency of charge transporting layer. Moreover, we estimated the electronic trap density in perovskite layer by measuring dark current-voltage profiles of the electron-only devices with a structure of FTO/TiO₂/perovskite/PCBM/Ag electrode.^[45] Figure 2c depicts the dark current-voltage curves of the corresponding samples, which include an Ohmic regime, a trap-filled limited regime (TFL) and a trap-free space charge limit current (SCLC) regime (Child). The trap density can be deduced from the trap-filled limit voltage (V_{TFL}) that is corresponding to the onset voltage of the trap-filled limit region, as shown in the following equation.^[8]

$$N_{\text{trap}} = \frac{2\epsilon_0\epsilon_r V_{TFL}}{ed^2} \quad (1)$$

where ϵ_0 is the vacuum permittivity, ϵ_r is the relative dielectric constant, e is the charge constant, and d is the thickness of the perovskite film. It is found that the statistic trap density significantly decrease from 3.02×10^{16} to 2.69×10^{16} , 1.95×10^{16} , and $9.7 \times 10^{15} \text{ cm}^{-3}$ for the control and SP1, SP2, SP3 passivated devices (Figure 2d), respectively, illustrating the SP3 with a good control of electron density distribution is more efficient for eliminating those ion-induced trap states in the hybrid perovskite materials.

To further study the passivation effect on the device photovoltaic performance, we fabricated the perovskite solar cells with an invert planar configuration of FTO glass/NiO_x/MAPbI₃ Perovskite (without or with D- π -A molecules)/PCBM/BCP/Ag (Figure 3a), and Figure S10, Supporting Information, depicts the cross-section SEM image of the optimized SP3 passivated devices. The photovoltaic parameters of the champion devices based on different perovskite absorbers are shown in Table 1, and

Table 1. Photovoltaic performance of the champion devices for the corresponding PSCs.

PSCs	V_{oc} [V]	J_{sc} [mA cm ⁻²]	J_{sc}^a [mA cm ⁻²]	FF [%]	PCE [%]	PCE ^b [%]
Control	1.066	22.50	22.62	77.20	18.52	18.19
SP1	1.075	22.53	22.76	77.42	18.75	18.48
SP2	1.094	22.63	22.83	77.82	19.27	18.91
SP3	1.146	22.69	22.88	78.55	20.43	20.09

^a) Calculated J_{sc} from the IPCE spectrum; ^b) The steady-state PCE was measured under constant voltage of the maximum power point.

the corresponding J - V curves are plotted in Figure 3b. The control devices give the best PCE of 18.52%, with a V_{oc} of 1.066 V, J_{sc} of 22.50 mA cm⁻², and fill factor (FF) of 77.20%. On the contrary, SP3 passivated devices exhibit enormous improvement of 80 mV in V_{oc} and present the best PCE up to 20.43%, showing a V_{oc} of 1.146 V, J_{sc} of 22.69 mA cm⁻² and FF of 78.55%. Meanwhile, the SP1- and SP2-based solar cells just exhibit a slight enhancement in V_{oc} , with the best performance of 18.75% (V_{oc} of 1.075 V) and 19.27% (V_{oc} of 1.094 V), respectively. We attribute such great enhancement of V_{oc} to the minimized electronic trap density in the active layer of SP3 passivated devices. Moreover, the statistic efficiency distributions of PSCs based on 16 devices in a batch are plotted in Figure S11, Supporting Information, and the corresponding average photovoltaic parameters are also shown in Table S2, Supporting Information.

To ensure the reliability of the device performance, we tracked the steady-state PCE under constant voltage of the maximum power point (V_{max}) for about 300 s (Figure 3c). The V_{max} for the control as well as SP1, SP2, and SP3-containing perovskite devices were calculated to be 0.88, 0.89, 0.92, and 0.99 V, respectively. The stabilized efficiency of 20.09% could be achieved for the SP3 passivated solar cell, which greatly consists of the obtained PCE from the J - V measurements. On the other side, the internal photo-current efficiency (IPCE) spectrums for the corresponding devices are depicted in Figure 3d, suggesting that the incorporation of D- π -A molecules has little influence on the charge extraction efficiency of PSCs. Meanwhile, the integrated current density were calculated to be 22.62, 22.76, 22.83, and 22.88 mA cm⁻² for the control and SP1-, SP2-, SP3-passivated devices, respectively, which are quite in agreement with the J_{sc} obtained from the J - V characterization within a deviation less than 1%.

Except for the abovementioned, we carried out the dark-current analysis to study the leakage current formed by carrier recombination in the solar cells. As shown in Figure 3e, the SP3-passivated device exhibits a relatively lower saturation current density ($J_0 = 7.26 \times 10^{-10}$ mA cm⁻²) compared to that of the control ($J_0 = 7.75 \times 10^{-9}$ mA cm⁻²), SP1 ($J_0 = 5.13 \times 10^{-9}$ mA cm⁻²) passivated and SP2 passivated ($J_0 = 2.69 \times 10^{-9}$ mA cm⁻²) ones. As known, a lower J_0 leads to less charge recombination as well as a larger V_{oc} in the solar cell. Additionally, we conduct the transient photovoltage (TPV) measurement to characterize the charge recombination lifetime of the PSCs (Figure S12, Supporting Information). The device with SP3 passivation show a substantially slower decay of TPV ($\tau = 3.32$ μ s) than that of the pristine one ($\tau = 1.75$ μ s), suggesting that the charge recombination in perovskite devices is effectively suppressed by the passivation effect of SP3.

To figure out the effect of D- π -A molecules on the stability of perovskite films, we also measured the static contact angle with water of different samples (Figure 4a-d). The contact angles of perovskite films increase significantly after introducing the hydrophobic D- π -A molecules. Besides we found that SP3 is more effective for preventing the permeation of moisture into the perovskite crystal, which may be attributed to the minimized content of metallic Pb cluster on perovskite surface resulting in less halide vacancies acting as the diffusion channel of water or oxygen molecules.^[46] Moreover, we also exposed the perovskite films in ambient air, and measured their X-ray diffraction (XRD) patterns after aging for 10 days. As shown in

Figure 4e, the SP3 passivated film displays a comparatively lower content of PbI₂ phase, indicating a less crystalline decomposition of MAPbI₃ perovskite in contrast to the fresh samples. The air stability test of the PSCs devices encapsulated was also carried out in the ambient air, and the decay curves were recorded in Figure 4f. It is noted that the SP3-treated perovskite device retains 86% of its initial PCE after 30 days aging, while the control, SP1-passivated, and SP2-passivated cells present more severe degradation with a PCE decrease of 37%, 29%, and 24%, respectively, testing under the same condition.

In summary, we first propose a strategy to optimize the defect passivation process in hybrid perovskite layer via systematically controlling the electron density distribution of passivation molecules with a donor- π -acceptor structure. Theoretical calculation and experimental studies demonstrate that the passivation effect increases with the polarity of the D- π -A molecules. Increase of donating ability will significantly intensify the coordination effect between electron-withdrawing functional group and under-coordinated Pb²⁺ cations, leading to a superiority on minimizing the trap states and suppressing the non-radiative recombination in perovskite absorber. By adding strong electron donating group (N,N-dibutylamine) to the D- π -A structure (SP3), we achieve a significant increase of 80 mV in V_{oc} and the PCE of 20.43% for the invert planar perovskite device, as compared with a PCE of 18.52% by the cell without SP3. In addition, the hydrophobic character of D- π -A molecules remarkably improves the moisture stability of perovskite films and devices. This work also gives a new route to design the passivation molecule for highly efficient and stable perovskite solar cells based on controlling the electron density distribution of other organic electron push-pull structures such as D-A- π -A or A- π -D- π -A to an overall passivation for the ionic defects and improve both efficiency and stability of perovskite solar cells.

3. Experimental Section

Devices Fabrication: The FTO-coated glasses were etched with zinc powder and 1 M HCl to obtain patterned substrates. The patterned glasses were then sonicated with detergent, deionized water, ethanol, and acetone for 20 min, respectively. After being dried by the N₂ flow, the substrates were treated with UV plasma for 20 min to remove the organic residues. Then, the NiO precursor solution comprising 30 mL nickel acetylacetonate (with 15 mol% magnesium acetate tetrahydrate and 5 mol% lithium acetate) in acetonitrile/ethanol (95:5 v:v) was sprayed onto the pre-heated FTO-coated glasses within 20 min at 570 °C by an air nozzle, and the substrates were kept at 570 °C for another 30 min to form hole transporting layer of NiO_x (about 20 nm in thickness). After that, the substrates were transferred into a N₂ atmosphere after cooling down to 100 °C. The perovskite precursor solution which was composed of 1.3 M PbI₂ and CH₃NH₃I (1:1/n:n) in DMF and DMSO (5:1 v:v) was stirred at 60 °C overnight, and the resulting solution was spin-coated on the NiO_x layer consecutively at 1000 and 5000 rpm for 10 and 20s, respectively. After that, 800 μ L chlorobenzene without or with D- π -A molecules (10⁻⁴ M) was dripped quickly onto the perovskite precursor about 8 s after the first spin-coating step, and the substrate was annealed at 100 °C for 20 min. Then, a layer of PCBM (80 nm) was deposited by spin-coating 20 mg mL⁻¹ PCBM chlorobenzene solution on the perovskite film at 1000 rpm for 30s and dried at 70 °C for 10 min. Finally, bathocuproine (BCP) was coated on PCBM by depositing 150 μ L as-prepared dispersion drop by drop at 6000 rpm for 30 s, and annealing at 70 °C for 5 min. All of these processes were conducted in the N₂-protected glove box with the contents of O₂ and H₂O less than

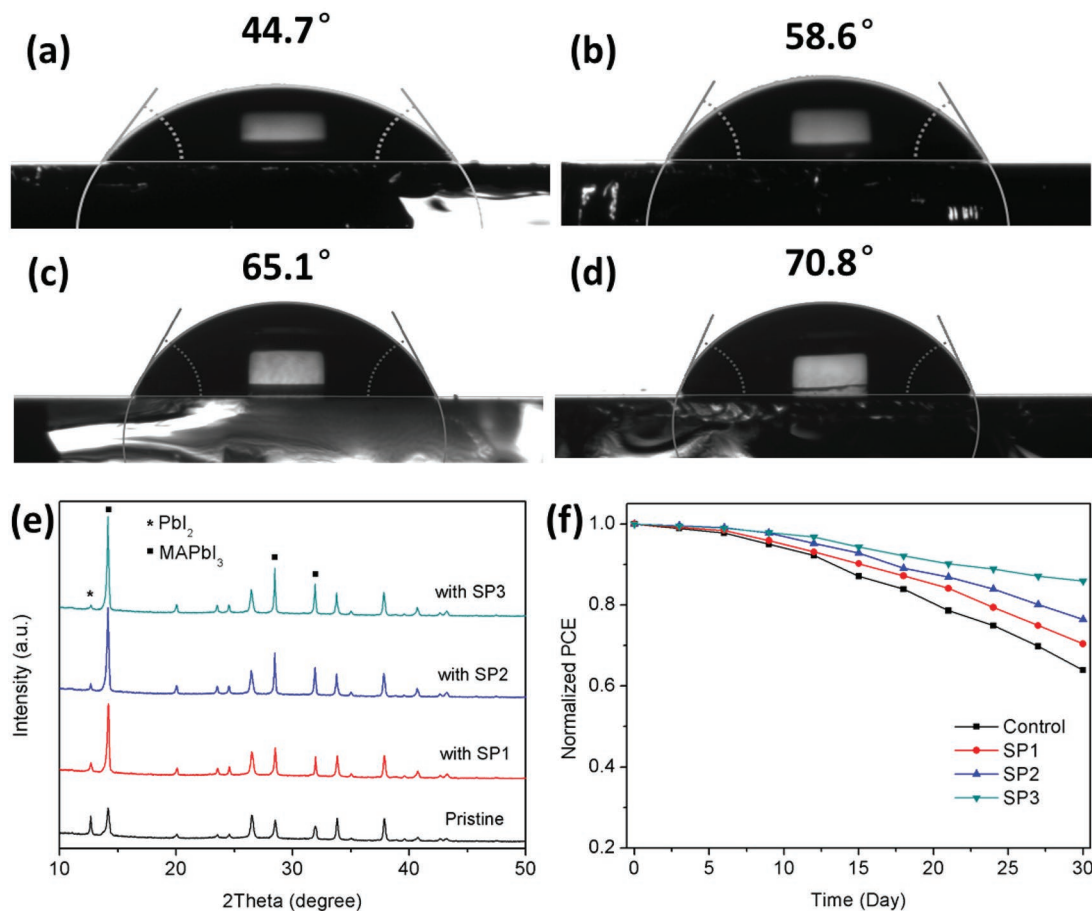


Figure 4. Static contact angle measurements with water on top of the perovskite films: a) pristine, b) SP1 passivation, c) SP2 passivation, and d) SP3 passivation. e) XRD patterns of the corresponding perovskite films aging in air with the relative humidity of 30% for 10 days. f) The PCE decays of the corresponding PSCs under ambient air with a relative humidity about 30% with encapsulation.

0.01 ppm. At last, the 100 nm silver electrode was formed by thermal evaporation under high vacuum (lower than 2×10^{-4} Pa).

Film Characterization: Field emission scanning electron microscopy (FESEM, Sirion 200, FEI & Oxford) was used to observe the morphology of the as-obtained products. Fluorescence spectra were measured with a Horiba Fluoromax-4 fluorescence spectrometer. The time-resolved photoluminescence decay was recorded by Horiba Fluorolog-3 Time Correlated Single Photon Counting system with the excitation wavelength at 440 nm. X-ray photoelectron spectroscopic (XPS) analysis was carried out on a Kratos AXIS Ultra DLD spectrometer by using an Al K α X-ray source. The XRD patterns were measured on a Rigaku Ultima IV powder X-ray diffractometer using Cu K α radiation. Time-of-flight secondary-ion mass spectrometry (ToF-SIMS) measurements were performed using the focused ion beam ToF-SIMS spectrometer (GAIA3 GMU Model 2016, Czech). A 30 keV Bi⁺ ion beam was used as the primary ion beam to peel the samples with an analysis area of $5 \times 5 \mu\text{m}^2$. UV-vis absorption spectra of perovskite film samples were recorded by a Shimadzu UV 2450 spectrometry. The linear voltage sweep mode employed to investigate the space charge limit current (SCLC) plots and dark *J-V* curves was performed on a multi-functional electrochemical analysis instrument (Zahner, Germany), with a constant step voltage of 20 mV. The static contact angle with water droplet was conducted on DSA 100 contact angle measuring device (KRUS GmbH, Germany).

Photovoltaic Measurement: *J-V* curves of the PSCs were measured with a digital source meter (Keithley 2400) under simulated solar illumination at 100 mW cm^{-2} (AM 1.5G). The light source was determined by a standard silicon reference cell (Wacom Denso Co., Japan). The measurement

was conducted by reverse (from 1.2 to -0.2 V) or forward (from -0.2 to 1.2 V) scan where scanning was conducted from -0.2 to +1.2 V. The step voltage and delay time were fixed at 10 mV and 30 ms, respectively.^[47] Monochromatic incident photo-to-current conversion efficiency spectra measurements were characterized employing a monochromatic incident light of 1×10^{16} photons cm^{-2} with direct current mode.

Quantum Chemical Calculations: Calculation details are presented as follows: Density functional theory (DFT) calculations were conducted on the Gaussian 09 program by using B3LYP and the all-electron double- ξ valence basis sets of 6-31G*. Geometry optimizations of the organic dyes were performed with default spin mode at the gas phase. Vibrational frequency calculations were also employed to make sure the optimized structure of dye molecule has no imaginary frequency.

Supporting Information

Supporting Information is available from the Wiley Online Library or from the author.

Acknowledgements

T.W. and Y.W. contributed equally to this work. This work was partially supported by the National Natural Science Foundation of China (grant numbers 11574199 and 11674219), the New Energy and Industrial

Technology Development Organization (NEDO, Japan), the Program for Professor of Special Appointment (Eastern Scholar) at Shanghai Institutions of Higher Learning, Natural Science Foundation of Shanghai (17ZR1414800).

Conflict of Interest

The authors declare no conflict of interest.

Keywords

defect passivation, donor- π -acceptor molecules, electron density distribution, perovskite solar cells

Received: December 5, 2018

Revised: January 29, 2019

Published online:

- [1] W. Chen, Y. Wu, Y. Yue, J. Liu, W. Zhang, X. Yang, H. Chen, E. Bi, I. Ashraf, M. Gratzel, L. Han, *Science* **2015**, *350*, 944.
- [2] W. S. Yang, J. H. Noh, N. J. Jeon, Y. C. Kim, S. Ryu, J. Seo, S. I. Seok, *Science* **2015**, *348*, 1234.
- [3] F. Xie, C.-C. Chen, Y. Wu, X. Li, M. Cai, X. Liu, X. Yang, L. Han, *Energy Environ. Sci.* **2017**, *10*, 1942.
- [4] N. J. Jeon, J. H. Noh, W. S. Yang, Y. C. Kim, S. Ryu, J. Seo, S. I. Seok, *Nature* **2015**, *517*, 476.
- [5] D. P. McMeekin, G. Sadoughi, W. Rehman, G. E. Eperon, M. Saliba, M. T. Höraantner, A. Haghighirad, N. Sakai, L. Korte, B. Rech, M. B. Johnston, L. M. Herz, H. J. Snaith, *Science* **2016**, *351*, 151.
- [6] G. Xing, N. Mathews, S. Sun, S. S. Lim, Y. M. Lam, M. Grätzel, S. Mhaisalkar, T. C. Sum, *Science* **2013**, *342*, 344.
- [7] S. D. Stranks, G. E. Eperon, G. Grancini, C. Menelaou, M. J. P. Alcocer, T. Leijtens, L. M. Herz, A. Petrozza, H. J. Snaith, *Science* **2013**, *342*, 341.
- [8] Q. Dong, Y. Fang, Y. Shao, P. Mulligan, J. Qiu, L. Cao, J. Huang, *Science* **2015**, *347*, 967.
- [9] M. Liu, M. B. Johnston, H. J. Snaith, *Nature* **2013**, *501*, 395.
- [10] A. Mei, X. Li, L. Liu, Z. Ku, T. Liu, Y. Rong, M. Xu, M. Hu, J. Chen, Y. Yang, M. Grätzel, H. Han, *Science* **2014**, *345*, 295.
- [11] X. Li, D. Bi, C. Yi, J.-D. Décoppet, J. Luo, S. M. Zakeeruddin, A. Hagfeldt, M. Grätzel, *Science* **2016**, *353*, 58.
- [12] H. Chen, F. Ye, W. Tang, J. He, M. Yin, Y. Wang, F. Xie, E. Bi, X. Yang, M. Grätzel, L. Han, *Nature* **2017**, *550*, 92.
- [13] N. J. Jeon, H. Na, E. H. Jung, T.-Y. Yang, Y. G. Lee, G. Kim, H.-W. Shin, S. I. Seok, J. Lee, J. Seo, *Nat. Energy* **2018**, *3*, 682.
- [14] T. Niu, J. Lu, R. Munir, J. Li, D. Barrit, X. Zhang, H. Hu, Z. Yang, A. Amassian, K. Zhao, S. F. Liu, *Adv. Mater.* **2018**, *30*, 1706576.
- [15] Y. Lin, L. Shen, J. Dai, Y. Deng, Y. Wu, Y. Bai, X. Zheng, J. Wang, Y. Fang, H. Wei, W. Ma, X. C. Zeng, X. Zhan, J. Huang, *Adv. Mater.* **2017**, *29*, 1604545.
- [16] Y. Wu, F. Xie, H. Chen, X. Yang, H. Su, M. Cai, Z. Zhou, T. Noda, L. Han, *Adv. Mater.* **2017**, *29*, 1701073.
- [17] F. Ye, H. Chen, F. Xie, W. Tang, M. Yin, J. He, E. Bi, Y. Wang, X. Yang, L. Han, *Energy Environ. Sci.* **2016**, *9*, 2295.
- [18] F. Ye, W. Tang, F. Xie, M. Yin, J. He, Y. Wang, H. Chen, Y. Qiang, X. Yang, L. Han, *Adv. Mater.* **2017**, *29*, 1701440.
- [19] Y. Peng, Y. Cheng, C. Wang, C. Zhang, H. Xia, K. Huang, S. Tong, X. Hao, J. Yang, *Org. Electron.* **2018**, *58*, 153.
- [20] Y. Wu, X. Yang, W. Chen, Y. Yue, M. Cai, F. Xie, E. Bi, A. Islam, L. Han, *Nat. Energy* **2016**, *1*, 16148.
- [21] K. T. Cho, S. Paek, G. Grancini, C. Roldan-Carmona, P. Gao, Y. Lee, M. K. Nazeeruddin, *Energy Environ. Sci.* **2017**, *10*, 621.
- [22] M. Cai, N. Ishida, X. Li, X. Yang, T. Noda, Y. Wu, F. Xie, H. Naito, D. Fujita, L. Han, *Joule* **2018**, *2*, 296.
- [23] C. Wang, C. Zhang, S. Wang, G. Liu, H. Xia, S. Tong, J. He, D. Niu, C. Zhou, K. Ding, Y. Gao, J. Yang, *Sol. RRL* **2018**, *2*, 1700209.
- [24] E. Bi, H. Chen, F. Xie, Y. Wu, W. Chen, Y. Su, A. Islam, M. Gratzel, X. Yang, L. Han, *Nat. Commun.* **2017**, *8*, 15330.
- [25] Y. Yuan, J. Huang, *Acc. Chem. Res.* **2016**, *49*, 286.
- [26] W. Zhou, Y. Zhao, X. Zhou, R. Fu, Q. Li, Y. Zhao, K. Liu, D. Yu, Q. Zhao, *J. Phys. Chem. Lett.* **2017**, *8*, 4122.
- [27] X. Zheng, B. Chen, J. Dai, Y. Fang, Y. Bai, Y. Lin, H. Wei, X. C. Zeng, J. Huang, *Nat. Energy* **2017**, *2*, 17102.
- [28] Y. Guo, J. Ma, H. Lei, F. Yao, B. Li, L. Xiong, G. Fang, *J. Mater. Chem. A* **2018**, *6*, 5919.
- [29] N. De Marco, H. Zhou, Q. Chen, P. Sun, Z. Liu, L. Meng, E.-P. Yao, Y. Liu, A. Schiffer, Y. Yang, *Nano Lett.* **2016**, *16*, 1009.
- [30] A. Abate, M. Saliba, D. J. Hollman, S. D. Stranks, K. Wojciechowski, R. Avolio, G. Grancini, A. Petrozza, H. J. Snaith, *Nano Lett.* **2014**, *14*, 3247.
- [31] X. Li, C.-C. Chen, M. Cai, X. Hua, F. Xie, X. Liu, J. Hua, Y.-T. Long, H. Tian, L. Han, *Adv. Energy Mater.* **2018**, *8*, 1800715.
- [32] N. K. Noel, A. Abate, S. D. Stranks, E. S. Parrott, V. M. Burlakov, A. Goriely, H. J. Snaith, *ACS Nano* **2014**, *8*, 9815.
- [33] S. Zhang, X. Yang, Y. Numata, L. Han, *Energy Environ. Sci.* **2013**, *6*, 1443.
- [34] M. Liang, J. Chen, *Chem. Soc. Rev.* **2013**, *42*, 3453.
- [35] H.-Y. Yang, Y.-S. Yen, Y.-C. Hsu, H.-H. Chou, J. T. Lin, *Org. Lett.* **2010**, *12*, 16.
- [36] J. Mao, N. He, Z. Ning, Q. Zhang, F. Guo, L. Chen, W. Wu, J. Hua, H. Tian, *Angew. Chem., Int. Ed.* **2012**, *51*, 9873.
- [37] Y. Numata, I. Ashraf, Y. Shirai, L. Han, *Chem. Commun.* **2011**, *47*, 6159.
- [38] Y. Cui, Y. Wu, X. Lu, X. Zhang, G. Zhou, F. B. Miaphe, W. Zhu, Z.-S. Wang, *Chem. Mater.* **2011**, *23*, 4394.
- [39] S. Zhang, A. Islam, X. Yang, C. Qin, K. Zhang, Y. Numata, H. Chen, L. Han, *J. Mater. Chem. A* **2013**, *1*, 4812.
- [40] Y. Wu, W. Zhu, *Chem. Soc. Rev.* **2013**, *42*, 2039.
- [41] K. Kurotobi, Y. Toude, K. Kawamoto, Y. Fujimori, S. Ito, P. Chabera, V. Sundström, H. Imahori, *Chem. - Eur. J.* **2013**, *19*, 17075.
- [42] D. Wei, F. Ma, R. Wang, S. Dou, P. Cui, H. Huang, J. Ji, E. Jia, X. Jia, S. Sajid, A. M. Elseman, L. Chu, Y. Li, B. Jiang, J. Qiao, Y. Yuan, M. Li, *Adv. Mater.* <https://doi.org/10.1002/adma.201707583>.
- [43] W. Zhang, S. Pathak, N. Sakai, T. Stergiopoulos, P. K. Nayak, N. K. Noel, A. A. Haghighirad, V. M. Burlakov, D. W. deQuilettes, A. Sadhanala, W. Li, L. Wang, D. S. Ginger, R. H. Friend, H. J. Snaith, *Nat. Commun.* **2015**, *6*, 10030.
- [44] W. Huang, S. Sadhu, S. Ptasinska, *Chem. Mater.* **2017**, *29*, 8478.
- [45] H. Tan, A. Jain, O. Voznyy, X. Lan, F. P. G. de Arquer, J. Z. Fan, R. Quintero-Bermudez, M. Yuan, B. Zhang, Y. Zhao, F. Fan, P. Li, L. N. Quan, Y. Zhao, Z.-H. Lu, Z. Yang, S. Hoogland, E. H. Sargent, *Science* **2017**, *355*, 722.
- [46] L. Liu, S. Huang, Y. Lu, P. Liu, Y. Zhao, C. Shi, S. Zhang, J. Wu, H. Zhong, M. Sui, H. Zhou, H. Jin, Y. Li, Q. Chen, *Adv. Mater.* **2018**, *30*, 1800544.
- [47] M. Yin, F. Xie, X. Li, Y. Wu, X. Yang, F. Ye, Y. Wang, J. He, W. Tang, E. Bi, H. Chen, L. Han, *Appl. Phys. Express* **2017**, *10*, 076601.